Investigation of Intrinsic Point Defects in Metals by Nuclear Quadrupole Double Resonance *

M. Notter [a], K. Konzelmann [b], G. Majer [b], and A. Seeger [a, b]

[a] Universität Stuttgart, Institut für Theoretische und Angewandte Physik, Pfaffenwaldring 57/VI, D-70569 Stuttgart, Germany
[b] Max-Planck-Institut für Metallforschung, Institut für Physik, Heisenbergstr. 1, D-70569 Stuttgart, Germany

Z. Naturforsch. **49a**, 47–64 (1994); received October 26, 1993

The paper reviews the principal features of the Nuclear Quadrupole Double Resonance (NQDOR) technique, with particular emphasis on its application to the investigation of imperfections in cubic metals. NQDOR permits measurements of the electric field gradients (EFG) at quadrupole-moment-carrying nuclei in the neighbourhood of point defects and thus to obtain "fingerprints" of these defects. An NQDOR facility set-up at the Max-Planck-Institut für Metallforschung in Stuttgart is described. It has been used to study the intrinsic defects introduced into Cu and dilute Cu/Be alloys by low-temperature irradiation with electrons or protons or by cold-work. It is shown that all well-resolved irradiation-induced EFG observed in the present work are due to one kind of defect only, which is identified as the ⟨100⟩ dumbbell self-interstitial. When considered together with measurements of the electrical resistivity on the same specimens, the annealing behaviour of the NQDOR lines supports the so-called two-interstitial model of radiation damage in face-centred cubic metals rather than the one-interstitial model.

Key words: Nuclear quadrupole double resonance; Self-interstitials; Vacancies; Radiation damage; Intrinsic point defects in copper.

1. Introduction

Since the early 1950s the behaviour of intrinsic point defects (vacancies and self-interstitials) in metals under non-equilibrium conditions has been investigated extensively [1, 2], prompted by interest in the changes of properties of materials caused by irradiation with energetic particles. Nevertheless, many observations in this field are still not well understood.

Especially the identification of intrinsic point defects in metals is still under discussion. This is due, on the one hand, to the wide variety of complicating effects such as trapping of mobile defects at impurities, formation of defect clusters etc. and, on the other hand, to the fact that only under very special conditions can point defects be studied directly by imaging methods (e.g., field ion microscopy, electron microscopy, tunnelling microscopy).

Most of our present knowledge on intrinsic point defects in metals was obtained by methods such as electrical resistance measurements, which do not allow us to distinguish between different types of lattice defects or which require fairly high defect concentrations (such as, e.g., X-ray scattering), or by means of special probes (as used in, e.g., perturbed angular correlation or Mößbauer studies). **N**uclear **Q**uadrupole **Do**uble **R**esonance (NQDOR) [3–7], the topic of the present paper, is a technique *not* involving external probes that nevertheless permits the characterization of specific defects in crystals even in atomic concentrations as low as a few ppm. However, up to now NQDOR has been applied to the study of point defects in metals only be three groups [4, 6, 8], presumably on account of the large experimental efforts required.

In simple crystal structures with cubic symmetry such as the **f**ace-**c**entred **c**ubic (fcc) or the **b**ody-**c**entred **c**ubic (bcc) lattice the traceless rank-two tensor V of the electric field gradient (EFG) vanishes at the lattice sites. The introduction of lattice defects disturbs this symmetry and hence give rise to EFG at nearby lattice sites. These EFG act on the quadrupole moments Q of the nuclei at these sites and lead to quadrupolar splittings of the nuclear energy levels. Unfortunately,

* Presented at the XIIth International Symposium on Nuclear Quadrupole Resonance, Zürich, Switzerland, July 19–23, 1993.

Reprint requests to Dr. G. Majer, Max-Planck-Institut für Metallforschung, Institut für Physik, Heisenbergstraße 1, D-70569 Stuttgart, Germany. FAX number: (0711) 689 10 10, e-mail: majer @ VAXPH.MPI-STUTTGART.MPG.DE.

0932-0784 / 94 / 0100-0047 $ 01.30/0. – Please order a reprint rather than making your own copy.

in the case of intrinsic point defects in metals these splittings, which clearly contain interesting information on the defects, cannot be studied by "pure" **N**uclear **Q**uadrupole **R**esonance (NQR) or by the observation of the satellites in high-field **N**uclear **M**agnetic **R**esonance (NMR) because of the low defect concentrations usually involved and the smallness of the NQR transition frequencies. NQDOR overcomes these difficulties by combining NMR in high magnetic fields with NQR in zero magnetic field. It allows us to search over a large frequency range for the quadrupolar splittings of minorities of nuclei.

Owing to different EFG on crystallographically distinct lattice sites in their vicinities, point defects of a given kind contribute several lines to the NQDOR spectrum, provided the magnitudes of the EFG correspond to the frequency range accessible to NQDOR. These lines can be used as "fingerprints" of the defects, as has been demonstrated for several metallic solutes in Al and Cu [6, 9]. In addition, within the so-called **D**ouble **I**rradiation **T**echnique (DIT) frequency regime, changes in the point defect concentration can be followed quantitatively (see Section 2.2). This feature is particularly important for studying the *recovery* of non-equilibrium concentrations of intrinsic defects introduced, e.g., by irradiation, cold-work, or quenching from high temperatures.

In metals, the recovery of intrinsic point defects during annealing at successively higher temperatures occurs in fairly distinct recovery stages that reflect the migration of defects with well-defined migration energies (comparable with fractional distillation but with the important difference that the defects vanish whereas in fractional distillation the separated fractions are available for subsequent investigation). A traditional nomenclature denotes the recovery stages by roman numbers which increase with increasing annealing temperature [1, 2]. In spite of strong efforts and much clarification the assignment of these stages to specific defect types has remained a point of discussion.

The characteristic features of NQDOR as outlined above allow us to obtain highly specific information on the intrinsic point defects responsible for the NQDOR lines including their behaviour during annealing treatments [10, 11]. In the present work NQDOR and electrical resistance were measured simultaneously on the *same* samples in order to relate the NQDOR results unambiguously to the conventional investigations of recovery processes.

In the first part of the paper (Sections 2 and 3) the principles and applicability of NQDOR will be reviewed, followed by some remarks on the "Solid Effect" in NQDOR and a description of the experimental set-up. The second part (Section 4) is devoted to the investigation of the properties of intrinsic point defects in metals by the NQDOR technique. This part includes a brief review of the earlier work in this area as well as a discussion of the need for further NQDOR experiments and for progress in the calculation of EFG.

2. The NQDOR Method

2.1 Basic Principles

Consider a crystal with cubic symmetry of the lattice sites that contains a low concentration of lattice defects. In such a crystal two spin systems can be defined, viz. the system A of the spins at sites which are so far from any lattice defect that their EFG's are negligibly small, and the system B of spins at nuclei with EFG-induced level splittings that are larger than the dipolar splitting due to the local magnetic field B_L. The basic weakness of zero-field NQR is that in it participate B nuclei only, which are far less numerous than the A nuclei.

The situation is radically different in NQDOR experiments. Here both spin systems are polarized in a high magnetic field (Figure 1). When the field is switched off adiabatically, the spin order is preserved, thus establishing a very low spin temperature T_{spin} that subsequently increases on a time scale given by the spin-lattice relaxation time in zero field, T_1^{zero}.

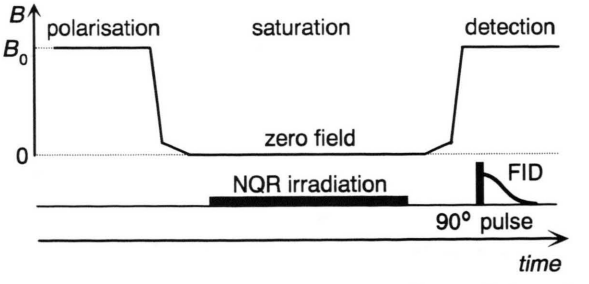

Fig. 1. The NQDOR cycle (B_0 = externally applied static magnetic field, FID = Free Induction Decay). In the present experiments the r.f. irradiation in zero field lasted about 180 ms. A waiting time of about 40 ms between reaching B_0 and magnetization detection was necessary in order to allow the eddy currents in the sample to die out.

Now a radio-frequency (r.f.) field is applied to the sample. When the frequency matches one of the quadrupolar splittings, the corresponding NQR transition is saturated, i.e., the spin temperature of the nuclei involved becomes infinite. If the two spin systems are coupled by "spin diffusion", the spin disorder associated with the high spin temperature of the B system is continuously transferred to the A system. Then the spin temperature of the entire sample increases in a time shorter than the "normal" T_1^{zero}. Even a small concentration of B nuclei may now lead to large changes in the spin temperature of the entire sample. After switching again to the high field, the remaining magnetization (which in high fields is proportional to $\beta = 1/k_B T_{\text{spin}}$, k_B = Boltzmann's constant) is detected by a 90° r.f. pulse.

The essential rôle of spin diffusion in NQDOR leads to the distinction between two frequency regimes, viz. the **S**ingle **I**rradiation **T**echnique (SIT) regime and the DIT regime. At *low* frequencies the spin temperatures of the two spin systems equalize by direct cross-relaxation between the B and the A system. In this frequency range r.f. irradiation with only one single frequency of low amplitude $B_1^{\text{NQR}} \ll B_L$ suffices. The cross-relaxation proceeds at least partly via nuclei that are neighbours in energy and space (i.e., step by step like on a staircase), thus depending on the distribution and level splittings of the participating nuclei [6]. E.g., the intensity of an NQDOR line may change due to changes in the surrounding defect pattern (e.g., neighbouring dislocations) without change in the concentration of the defects giving rise to the line. Hence in the SIT regime a quantitative analysis of the line intensities is feasible *only* if it can be verified that the cross-relaxation is not affected by other defects. An additional difficulty for quantitative work is that in the SIT regime the line intensities reflect the number of contributing nuclei weighted by the cross-relaxation, which is in most cases not well known.

At higher frequencies the cross-relaxation becomes ineffective. In this regime SIT would lead rather quickly to a new equilibrium state of the B system without detectable effects on the NQDOR signal. Therefore irradiation with large amplitude $B_1^{\text{NQR}} \approx B_L$ at *two* frequencies $\nu_q \pm \delta_m$ near the frequency ν_q of the quadrupolar transition ($2\pi\delta_m \approx \gamma B_L$, γ = magnetogyric ratio) is required in order to achieve continuous heating of all spins of the sample (DIT). In the DIT regime a quantitative analysis of the NQDOR line intensity is possible, as will be discussed in Section 2.2.

For nuclides with spin $I = 3/2$ such as ^{63}Cu and ^{65}Cu each EFG gives rise to only one quadrupolar transition frequency

$$\nu_q = e|Q||V_{zz}| \cdot \frac{(1+\eta^2/3)^{1/2}}{2h}, \tag{1}$$

where e is the elementary electric charge and h Planck's constant. In agreement with the standard practice the three principal components of the tensor of the electric field gradient, V_{ii}, are denoted in such a way that

$$|V_{zz}| \geq |V_{yy}| \geq |V_{xx}| \tag{2}$$

holds, so that the asymmetry ratio

$$\eta := (V_{xx} - V_{yy})/V_{zz} \tag{3}$$

obeys $0 \leq \eta \leq 1$.

In the case $\eta = 0$ Eq. (1) reads for ^{63}Cu with $Q = -(220 \pm 15) \cdot 10^{-31}$ m^2 [12]

$$\begin{aligned} \nu_q/\text{kHz} &= 2.660 \cdot 10^{-18} \cdot |V_{zz}|/\text{V} \cdot \text{m}^{-2} \\ &= 3.830 \cdot 10^{-21} \cdot \frac{|V_{zz}|}{e} \Big/ \text{cm}^{-3} \\ &= 2.584 \cdot 10^{4} \cdot |V_{zz}|/\text{a.u.}, \end{aligned} \tag{4}$$

where a.u. stands for atomic units (Rydberg units: $\hbar = 1$, electron mass $m_e = 1/2$, $e = \sqrt{2}$).

EFG acting on nuclides with spin $I = 5/2$ such as ^{27}Al give rise to *two* frequencies ν_q unless $\eta = 1$, i.e., unless $V_{xx} = 0$, $V_{yy} = -V_{zz}$ [13]. The ratio of the two frequencies (which varies monotonously between 2 in the case $\eta = 0$ to 1 in the case $\eta = 1$) contains information that is helpful in the attribution of EFG to sites (cf. Table 2).

Figure 2 illustrates the two frequency regimes mentioned above and the total frequency range available

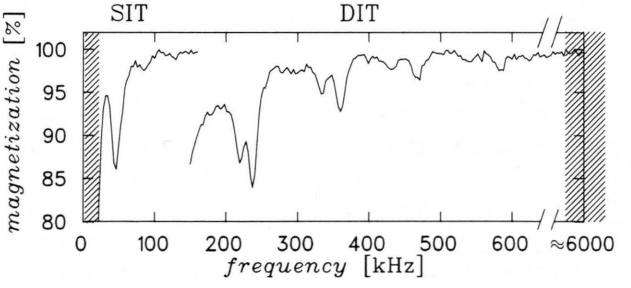

Fig. 2. NQDOR spectrum of Cu/200 ppm Be. The hatching denotes frequency regimes in which detection of NQDOR lines is difficult or impossible. Since Cu contains two isotopes with slightly different quadrupolar moments (cf. Table 1), each EFG gives rise to a line pair.

for detection of EFG in copper by the NQDOR technique. Very small EFG cannot be observed because of the dipolar absorption at low frequencies. On the other hand, with increasing frequency the search for lines becomes more and more laborious since the line widths are frequency-independent. A practical upper limit are frequencies of several MHz. A typical range of a frequency scan in Cu by SIT and DIT taken together is from 20 kHz to 6 MHz, corresponding to a ratio of about $3 \cdot 10^2$ between the largest and the smallest EFG detectable by NQDOR.

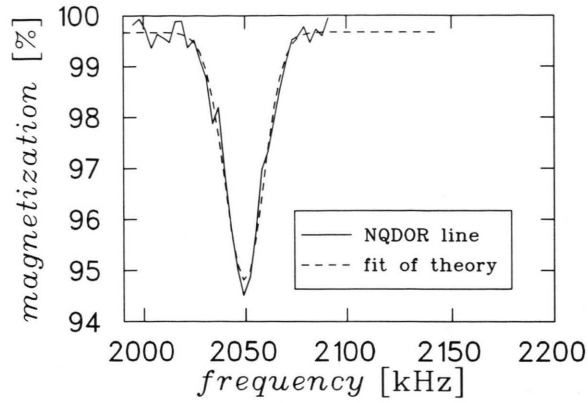

Fig. 3. Fit of the theoretical line-shape function [Eq. (5)] to the NQDOR line at 2.05 MHz in Cu/200 ppm Be.

2.2 Line Shape and Concentration Dependence in the DIT Regime

M. Minier [6] calculated the inverse spin temperature and thus the magnitude of the NMR signal after the NQDOR cycle under the assumption that spin diffusion is sufficiently fast to establish a single spin temperature for the dipolar system of the *entire* sample and that the r.f. irradiation is *symmetric* with respect to ν_q. The extension to r.f. irradiations that are *asymmetric* with respect to ν_q (the normal situation during scanning for NQR transitions) yields for the spin temperature in and near an NQDOR line in the DIT regime

$$\beta_d^{r.f.}(\tau) = \beta_d^{off}(\tau) \cdot \exp\left[-\frac{c_{d,B}}{c_d} \cdot 4\delta_m^2 \cdot \frac{W_q(\delta_c - \delta_m) \cdot W_q(\delta_c + \delta_m)}{W_q(\delta_c - \delta_m) + W_q(\delta_c + \delta_m)} \cdot \tau \right]. \quad (5)$$

In (5) δ_c denotes the difference between the frequency of the quadrupolar transition and the centre of the two irradiation frequencies, $\beta_d^{r.f./off}(\tau)$ the inverse spin temperatures with/without r.f. irradiation after the time τ in zero field, and $W_q(\delta_c \pm \delta_m)$ the transition probability of the quadrupolar transition at a given irradiation frequency including the shape function that takes the dipolar broadening into account. $c_{d,B}$ is the dipolar heat capacity of the B system (which is proportional to the defect concentration) and c_d that of the A system plus those B nuclei that are coupled to the A system by cross-relaxation. Figure 3 shows a fit of (5) to a measured line using a Gaussian function for $W_q(\delta_c \pm \delta_m)$. We see that (5) describes the sudden decrease of the nuclear magnetization at the wings of the line quite well.

At low defect concentrations c_d may be taken as constant. Under this condition DIT measurements allow us to follow quantitatively the changes of point defect concentrations during annealing. However, at defect concentrations exceeding several 100 ppm the contribution of the B nuclei enhance c_d significantly since their quadrupolar splittings are higher than the dipolar splitting of the A system [10]. Hence, for samples containing large fractions of nuclei with small quadrupolar splittings (due to, say, dislocations) a more sophisticated analysis is necessary.

2.3 Conditions for NQDOR Experiments on Metals

Metals must fulfill several conditions in order to permit NQDOR investigations. The nuclear quadrupole moment Q must be large enough to give rise to NQR transitions above the dipolar local splitting, and a reasonable NMR sensitivity is required. Furthermore, since the sensitivity of the NQDOR experiment is proportional to the ratio of the time available for irradiation in zero field ($\approx T_1^{zero}$) to the spin diffusion time T_{AB}, $T_2 \approx T_{AB} \ll T_1^{zero}$ must hold. The sample must not be ferromagnetic or superconducting in zero magnetic field. (Note that suppressing superconductivity by measuring at higher temperatures means lower sensitivity.)

Taken together, the preceding conditions are quite restrictive. The metallic elements with cubic crystal structure which satisfy them are listed in Table 1. In order for NQDOR to be applicable to non-cubic metals, the intrinsic quadrupolar splittings should not exceed the dipolar splitting. In most non-cubic metals the intrinsic quadrupolar splittings are of the order of magnitude 100 kHz or higher [14], so that this requirement is not satisfied. An exception might be ^{9}Be

Table 1. Spin I, nuclear quadrupole moment Q, and natural abundance of nuclides which fulfill the NQDOR conditions stated in the text (cubic metals only). The relative sensitivity for equal numbers of nuclei ($^1H = 1$) is used as measure for an acceptable NMR signal (relative sensitivity > 0.035). T_c is the temperature of the superconducting transition, [a] indicates existence of low-temperature phase transitions, [b] indicates that only little information is available on annealing behaviour at low temperatures. Q values taken from [12].

	^{7}Li[a,b]	^{23}Na[a,b]	^{27}Al	^{51}V	^{63,65}Cu	^{87}Rb[b]	^{93}Nb	^{181}Ta
I	3/2	3/2	5/2	7/2	3/2	3/2	9/2	7/2
Nat. abund. [%]	92.5	100	100	99.75	69.2, 30.8	27.8	100	100
Rel. NMR sens.	0.29	0.09	0.21	0.38	0.09, 0.11	0.18	0.48	0.036
$Q/(10^{-31}\,m^2)$	−40.1	109	140	210	−220, −204	132	−320	3170
Crystal structure	bcc	bcc	fcc	bcc	fcc	bcc	bcc	bcc
T_c/K	–	–	1.75	5.27	–	–	9.25	4.47

(hexagonal close-packed, $I = 3/2$, $Q = 53 \cdot 10^{-31}\,m^2$, $\nu_q \approx 30$ kHz [12, 14]), whose relative NMR sensitivity is rather small ($1.4 \cdot 10^{-2}$), though.

In the present context (quantitative investigation of intrinsic point defects) Cu is the best-suited metal since here considerable information on intrinsic point defects is available from other methods and since the controversial issues have been brought out clearly [1, 2]. The situation is similar in Al. However, all the NQDOR lines so far observed in this metal after low-temperature irradiation [10] lie in a much narrower frequency interval than those of copper, so that the probability that lines may overlap and cannot be distinguished is much higher.

From the point of view of the current discussion on properties of point defects, NQDOR experiments on niobium and tantalum are highly interesting, too. However, the fact that both metals are superconducting with rather high transition temperatures means that either one has to accept the lower sensitivity connected with elevated measuring temperatures as mentioned above or to make use of NQDOR in the rotating frame, which introduces other problems [15].

2.4 The Solid Effect

When two spins S and I with large energy splittings (characterized by the transition frequencies ν_S and ν_I; $\nu_S > \nu_I$) are weakly coupled by dipolar interactions, the mixing of the eigenfunctions leads to additional transitions at the sum and difference frequencies

$$\nu_{SE}^{\pm} = m\,\nu_S \pm n\,\nu_I, \tag{6}$$

where m and n are positive integers. This so-called **S**olid **E**ffect (SE) is well-known in **E**lectron **P**aramagnetic **R**esonance (EPR), where it is used, e.g., for the "dynamic spin polarization" of targets in nuclear physics [16]. The name originates from the fact that this effect can be only found in solid materials, whereas in fluids the dipolar coupling is averaged out by the fast motion of the spin carriers.

In the NQDOR Solid Effect S and I denote the spins of two nuclei of the B system with the quadrupolar transition frequencies ν_S and ν_I that are coupled by dipolar interaction. In this case *additional* lines may appear in the NQDOR spectrum at the sum and difference frequencies (6) that do not correspond to EFG values. Such lines were first found by Berthier and Minier [17] on dilute Al alloys. These authors calculated the transition probabilities for certain combinations of nuclei on different shells and developed special irradiation techniques which permitted the unambiguous identification of SE lines. All well-resolved SE lines so far reported correspond to $m = 1$ and $n = 1$. (An enhanced background absorption found on a dilute Al/300 ppm Ti alloy was attributed to spurious SE lines with $m + n \leq 5$ [17].) The Solid Effect can be of help in the assignment of measured EFG to definite shells (cf. Sect. 4.1) since the spins S and I must be neighbours in order to give sufficient dipolar coupling. In addition, solving (6) for ν_I may assist in separating overlapping low-frequency lines.

A very interesting situation arises if ν_I lies in the SIT and ν_S in the DIT regime. Then irradiation with a *single* frequency at the SE transition ν_{SE} suffices to couple the S levels and the dipolar A system via the I levels, which in turn are directly coupled to the dipolar A system via cross-relaxation (cf. Section 2.1). Such an irradiation does not saturate the S and I systems individually but leads to a saturation of the combined

system because of the SE between the S levels and the I levels. This means that $n^I_- \cdot n^S_- = n^I_+ \cdot n^S_+$ holds for the ν^+_{SE} transition and $n^I_+ \cdot n^S_- = n^I_- \cdot n^S_+$ for the ν^-_{SE} transition, where n^I and n^S denote the occupations of the I or the S levels, respectively, and the subscripts + or − refer to the upper or the lower levels. Although now the S spins are coupled to the A system, the SE line cannot be detected by continued irradiation with the *single* frequency ν_{SE} alone, since the S transition quickly reaches a new equilibrium state and no further absorption takes place. This equilibrium state is given by

$$\frac{n^I_+}{n^I_-} = \frac{n^S_-}{n^S_+} = \exp(\Delta E_I \, \beta_{zero}) \tag{7}$$

for the ν^+_{SE} transition and by

$$\frac{n^I_+}{n^I_-} = \frac{n^S_+}{n^S_-} = \exp(\Delta E_I \, \beta_{zero}) \tag{8}$$

for the ν^-_{SE} transition. Here ΔE_I denotes the quadrupolar splitting of the I levels, and β_{zero} the common inverse spin temperature of the A system and the I nuclei established by the direct cross-relaxation. Note that (7) describes a strong inversion while (8) describes a strong polarization in the occupation of the S levels. However, continuous heating of the A system, and hence a detectable effect on the magnetization, can be achieved by saturating the S levels by an additional irradiation at ν_S. This effect may be used for unambiguous identification of SE transitions as will be illustrated by an experimental example in Section 4.4.3.

A surprising fact is that, contrary to the above arguments, especially the ν^+_{SE} transition may be seen even in a *single*-frequency irradiation if its amplitude B_1^{NQR} is sufficiently high (comparable with B_L) (Figure 8). We have used this effect, first observed but not explained by Berthier and Minier [17], as an easy indicator for SE transitions (cf. Figure 8). We attribute it to the asymmetries of the S level occupancies. In both cases – polarization or inversion – the occupation difference is enhanced by the fact that the level splitting of the I nuclei is about an order of magnitude larger than that of the dipolar A system at *equal* spin temperature. Hence the strong inversion which is established during a single-frequency irradiation at ν^+_{SE} with a high B_1^{NQR} amplitude may prompt a self-amplification of weak field fluctuations at the S transition frequency due to induced emission, with similar effects as an additional r.f. irradiation at this frequency as described above.

3. The Experimental Set-up

Figure 4 gives an overview of the entire experimental set-up [8]. The NMR spectrometer is a home-built pulsed Fourier-transform device designed for measurements on solids using phase-sensitive quadrature detection in order to reduce channel asymmetries and dead time. A home-built field-cycling device switches the external field between zero and 0.68 T within 1.5 ms, employing a steady power of 30 kW and a pulsed power of 175 kW (500 A, 60 V steady, ±350 V during switching). The current is regulated by a battery of 120 power MOSFET IRF 542 in parallel connection and switched by bipolar power transistors (one battery with 40 BUT 35 and one with 8 SQD100A60 in parallel connection). The coil consists of 6 layers with about 30 turns per layer, wound from copper tubes with rectangular cross-sections, permitting water-cooling from inside. The coil has a bore diameter of 57 mm, an inductance of 750 μH, and a homogeneity of $6 \cdot 10^{-5}$ within 1 cm^3.

A home-built system permits computer-controlled r.f. irradiation at frequencies up to 6 MHz (Figure 5). An r.f. amplifier with a power of 50 W allows us to obtain B_1^{NQR} fields up to 2 mT. The system is capable of broad-band matching up to 1 MHz or narrow-band matching up to 6 MHz (extension to higher frequencies by adding a variable inductance is possible). B_1^{NQR} is kept constant within 2% even in the case of narrow-band matching by means of a regulation circuit which employes the voltage drop at a small resistor in series with the r.f. coil as a measure of the current through the coil. SIT irradiation and DIT irradiation [two frequencies with fixed frequency separation $2f_m$ at equal amplitudes $A \cos(2\pi f_m t) \cdot B \cos(2\pi f_{search} t)$, f_{search} = search frequency] are available as well as the special irradiation modes necessary to obtain SE lines [$A \cos(2\pi f_1 t) + B \cos(2\pi f_2 t)$; A, B, f_1, f_2 independently variable]. Noise, centre, and side-band suppression are better than 40 dB. The same r.f. coil is used for NMR detection and NQR irradiation in zero field, the two devices being decoupled by reed relays. R.f. coax relays would have provided better r.f. properties but their lifetimes proved too short for the present application.

All NQDOR measurements were performed at 2.1 K in order to give good sensitivity. The stability of the temperature regulation was $2 \cdot 10^{-3}$. When the cryostat was completely filled with liquid He, by pumping the cryostat 2.1 K were reached within one

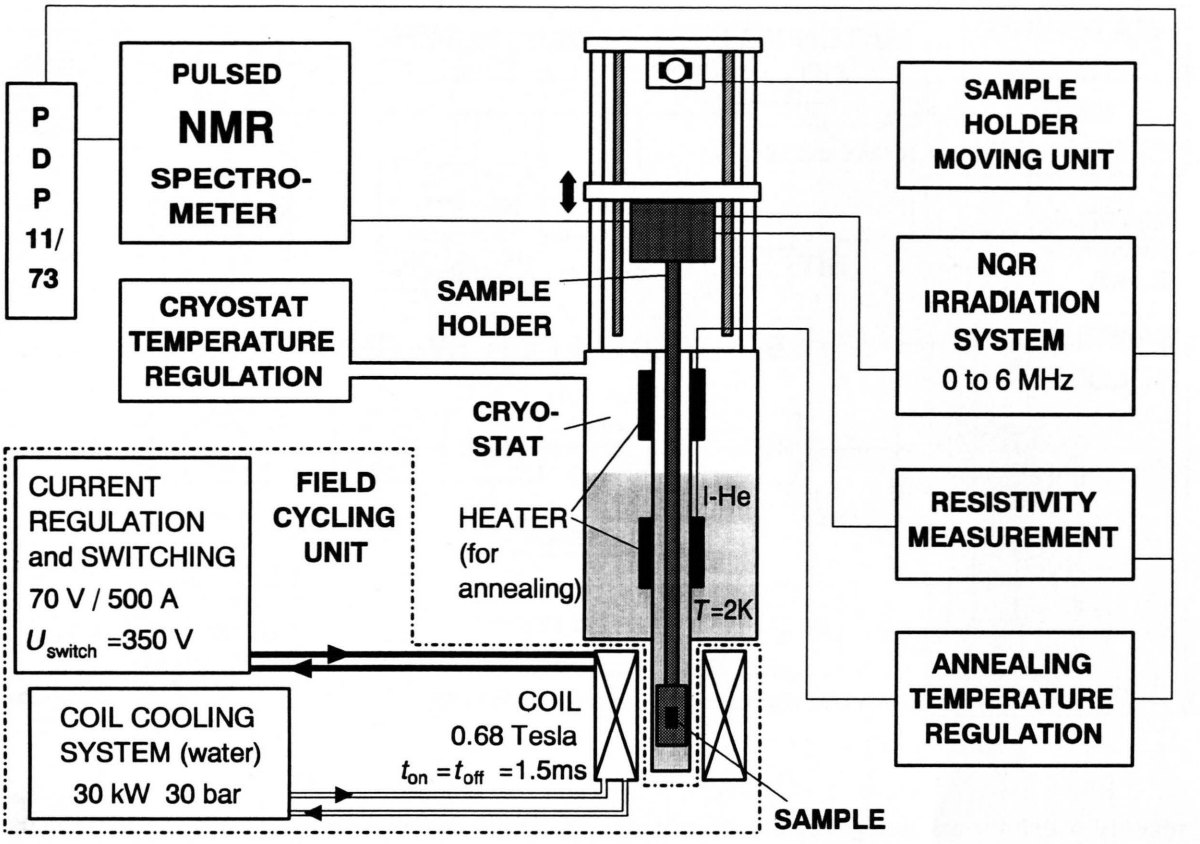

Fig. 4. Overview of the experimental set-up (for details see text).

hour. This temperature could be maintained for more than 24 hours in spite of the heating by eddy currents generated by the switching of the applied field.

Reaching our goal of a signal-to-noise ratio of about 200 (note that the strongest line of the cold-worked sample [cf. Fig. 13] yielded a decrease of the magnetization of only 5%) required careful and time-consuming elimination of the disturbances, especially in the signal detection, that came either from within the set-up or from outside sources.

Two ovens inside the cryostat permit annealing treatments. The sample is moved by a computer-controlled movement unit into the preheated oven and pushed back into the l-He reservoir after a predetermined time. The electrical resistivity is measured at 4.2 K by the usual four-point method with a sensitivity better than $10^{-9}\,\Omega$. For annealing at high temperatures (i.e., above 400 K) a special sample holder with integrated heater is used, which permits annealing up to 600 K.

4. NQDOR on Point Defects in Copper

4.1 General Background

The work of Redfield [4], who was the first to measure EFG (in dilute copper alloys) by means of NQDOR, and of Minier [6], who applied the method to dilute aluminium alloys, demonstrated that the observed spectra were characteristic for specific defect types. In 1977 and 1980 Minier et al. performed NQDOR measurements on powder samples of aluminium and copper that had been electron-irradiated at 30 K and 80 K, respectively [10, 11]. Their intention was to identify monovacancies in these metals by their NQDOR spectra and to determine their temperatures of migration. They found that irradiation with 3 MeV electrons leads to characteristics NQDOR spectra with well-resolved lines. In copper these lines remained nearly unchanged up to recovery stage III (i.e., up to just below room temperature), in which they

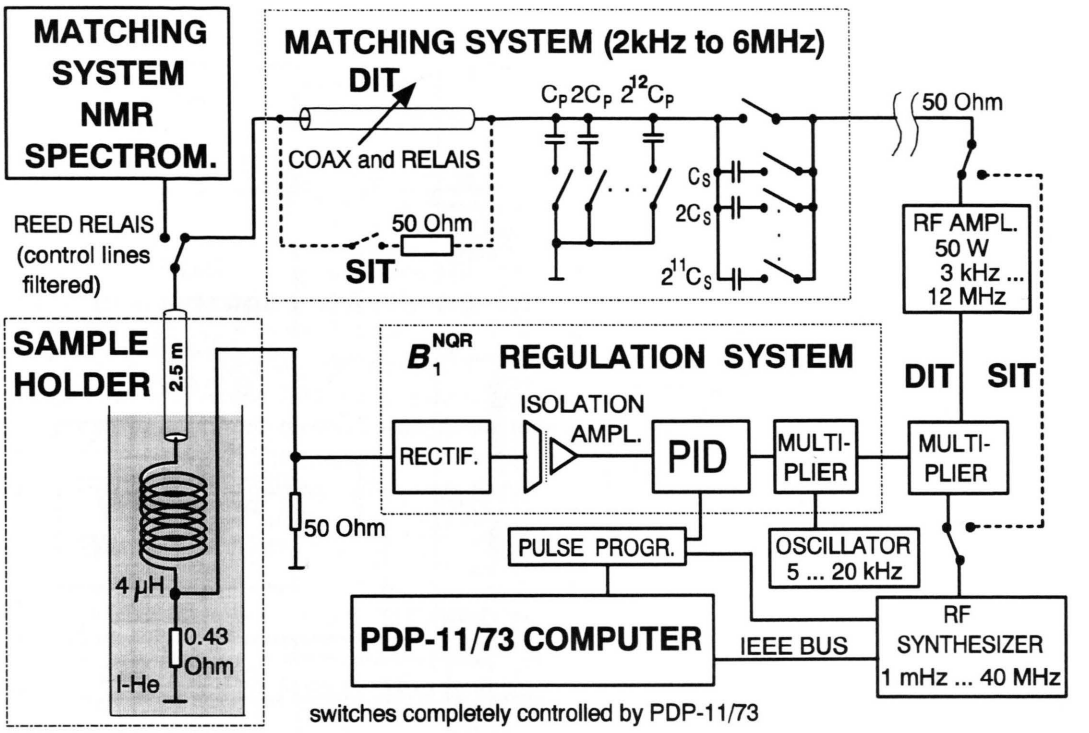

Fig. 5. The system for r.f. irradiation in zero field.

vanished within the measuring accuracy while about 1/7 of the irradiation-induced resistivity remained.

Since there is overwhelming experimental evidence that in all fcc metals Stage-III recovery is dominated by a defect–antidefect annihilation reaction, the above-mentioned NQDOR results allowed neither the definitive assignment of the observed lines to vacancies or self-interstitials (or to both) nor a decision on the nature of the defects migrating in recovery stage III. Nevertheless, Minier et al. assigned – in our view arbitrarily – all lines to monovacancies and concluded that in both metals investigated the defects migrating in Stage III were the monovacancies.

There are two approaches towards a definitive assignment of the observed lines. One of them is to calculate, preferably by ab-initio methods, the EFG acting on the nuclei in the neighbourhood of vacancies, self-interstitials etc. and to see which defect configurations account best for the experimental results. Among the potential strengths of this approach is that a given defect is characterised by several EFG; this means that it is unlikely that the theoretical predictions for different defects are so close that they cannot be distinguished experimentally. However, the computations on those metals on which the NQDOR experiments have concentrated so far, Cu and Al, have not proceeded far enough to solve the assignment problem. A brief status report on the theoretical achievements, suppressing some of the more technical questions, will be given in Section 4.2.

The alternative approach, followed in the present work, is to obtain additional experimental information. We may vary the defect pattern by introducing the defects in different ways, e.g., by e^- irradiation, ion irradiation, low-temperature cold-work, quenching from high temperatures, etc. One may also try to obtain further information from other measurements, say from the recovery of the electrical resistivity. The long-time strategy of our laboratory is to proceed along both the theoretical and the experimental avenue.

Fortunately, symmetry arguments and qualitative considerations allow us to reach quite a number of valuable conclusions without extensive computations. For a given type of defect (e.g., a vacant lattice site or a certain self-interstitial configuration) two general statements can be made, provided its EFG have the right magnitude to be detected by NQDOR. (i) Since

Table 2. Numbers of nuclei with equal EFG for vacancies, ⟨100⟩ dumbbell interstitials, and interstitials at octahedral sites in fcc metals. Entries in italics indicate that the corresponding EFG tensors are axially symmetric.

Shell number n	0	1	2	3	4	5	6
Vacancy	–	12	*6*	24	12	24	*8*
⟨100⟩ dumbbell	*2*	8+4	4+*2*	16+8	8+4	16+8	8
Octahedral site	–	*6*	*8*	24	–	24+*6*	24

neighbouring sites that can be transformed into each other by operations of the point symmetry group of the defects give rise to the same EFG (apart from different orientations of their principal axes), the line intensities reflect the number of sites in the various shells surrounding the defects. (ii) The likelihood that two NQDOR lines overlap becomes the larger the smaller the EFG is and the more nuclei with unequal EFG there are. This is the reason why dislocations and large defect clusters are expected to give rise not to sharp lines but to broad structureless absorption.

Having in mind the application to Cu and Al, we confine the following more specific remarks to fcc metals. Let us first consider monovacancies and make the generally accepted assumption that its point symmetry group is the octahedral group. We may then order the neighbouring sites in shells numbered according to increasing distance from the vacancy. If there is no lattice relaxation, the distance of the n^{th} shell is given by $(n/2)^{1/2}\, a_0$, where a_0 is the edge length of the elementary cube. The numbers of neighbours with the same EFG are listed in Table 2.

Considerable experimental and theoretical evidence indicates that the stable self-interstitial configuration in Cu and Al is the ⟨100⟩ dumbbell: An atom is removed from a lattice site, and two atoms are inserted symmetrically along one of the ⟨100⟩ directions. According to theory [18] and experiment [19], in Cu their distance from the vacated lattice site is about $0.6\, a_0$. If we take this site as the location of the self-interstitial, the shells of neighbouring atoms may be numbered the same way as for a vacancy. However, since the point symmetry is now tetragonal, in each shell the field gradients split into two groups whose members are in the ratio 2:1 (save for the 6^{th} shell, which contains the lattice sites in the ⟨111⟩ directions). The two "dumbbell atoms" may be considered as an additional zeroth shell containing two sites per interstitial.

For completeness we include in Table 2 also the so-called octahedral interstitial configuration, in which an atom has been inserted into a cube centre in such a way that the octahedral point symmetry is preserved. In this case the distances of the various shells from the inserted atom (again neglecting lattice relaxations) is given by $((2n-1)/4)^{1/2}\, a_0$ with the proviso that $n=4$ and $n=8$ are missing and that the shells $n=5$ and $n=9$ contain inequivalent sites with different EFG. Table 2 shows that the ratios 1:2:4 in the number of sites per shell occur both for the vacancy and the ⟨100⟩ dumbbell interstitial but not for the cube-centred interstitial. This means that by counting lines and comparing their intensities (note that this is meaningful only in the DIT regime, cf. Sect. 2.1) one cannot distinguish between the first two configurations unless one observes the ratio 1:8, a fact that apparently has been overlooked by Minier et al. [9–11]. (These authors erroneously believed that split self-interstitials such as the ⟨100⟩ dumbbell do not give rise to well defined NQDOR lines.)

4.2 Overview of Calculations on EFG Induced by Intrinsic Point Defects in Metals

Ab-initio calculations of EFG at nuclei in the neighbourhood of vacancies and interstitials in metals are a demanding task since the displacements of the ion cores from the regular lattice sites have to be taken into account (in the following we will refer to them as "lattice relaxation") and since the computations may not be confined to conduction and valence electrons but must include the inner shells. Reliable calculations have therefore been extremely rare. In the following we give a brief survey of what has been achieved mainly by the use of the density functional approximation.

Ponnambalam [20] calculated the EFG around vacancies in Al by means of a semi-empirical method (separate calculation of valence and size effects including corrections for antishielding), using a rather artificial approach to the lattice relaxations. The ab-initio computation of Drittler et al. [21] of the EFG at the nearest neighbours of vacancies and several substitutional impurities in copper based on KKR Green's functions neglects lattice relaxation altogether. If the accepted value for the quadrupole moment of ^{63}Cu is used ($Q=-(220\pm 15)\cdot 10^{-31}\,\text{m}^2$ [12] rather than $Q=-150\cdot 10^{-31}\,\text{m}^2$ used by Drittler et al.) the quadrupolar frequencies calculated by this approach are systematically too high. For the nearest neighbours of monovacancies in Cu the computations of

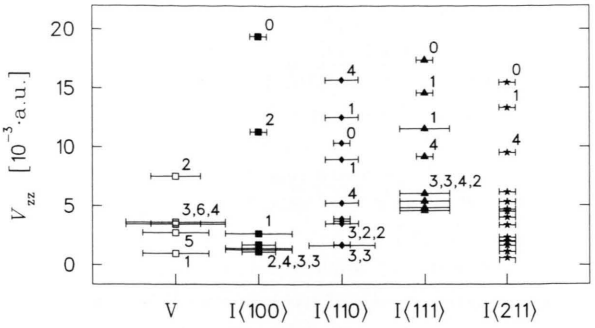

Fig. 6. Theoretical EFG values from an ab-initio pseudopotential computation on several intrinsic point defects in bcc Li [24, 25]. The EFG of vacancies and ⟨111⟩ self-interstitials were obtained from all-electron calculations, the others from valence-electron calculations. The lengths of the horizontal bars are proportional to the number of nuclei with equal EFG; the numbers at the data points are the shell numbers. The symmetry axes of the split interstitials are given in Miller indices.

Drittler et al. predict (6.0 ± 0.4) MHz (the error takes into account the uncertainty in Q only). Furthmüller [22] calculated the EFG generated by vacancies in Al using an ab-initio pseudopotential method that included self-consistent lattice relaxation. Without Sternheimer correction the largest of Furthmüller's EFG values (that at the nearest neighbours) is by about one order of magnitude lower than those measured on irradiated Al [10]; the others are too small to be detected by NQDOR. **L**inearized **A**ugmented-**P**lane-**W**ave (LAPW) calculations by Blaha et al. [23] on several hexagonal metals showed Sternheimer corrections to be unnecessary, so that we may conclude that Furthmüller's calculations do not support the assignment of the NQDOR lines of irradiated Al to monovacancies.

Theoretical results on EFG around vacancies and self-interstitials are available from all-electron supercell computations on bcc Li by Pawellek et al. [24, 25]. The EFG around split interstitials were found to be substantially higher than those around vacancies (see Figure 6). Unfortunately, NQDOR measurements on intrinsic point defects in bcc Li are hardly feasible due to the low-temperature phase transition of this metal, the recovery of the intrinsic point defects well below the l-N_2 temperature, and the small quadrupole moments of the stable isotopes ^{6}Li and ^{7}Li. All NQR transition frequencies as calculated from the EFG shown in Fig. 6 are situated below 100 kHz.

For self-interstitials in Al and Cu analogous results are not available. If we tentatively scale the results on vacancies and self-interstitials in Li with those on vacancies in Al [22], we are led to expect that the EFG of split self-interstitials in Al will have the right magnitude to explain the experimental results on e^--irradiated Al [10].

4.3 Samples and Experimental Procedure

4.3.1 Sample Preparation

Because of the skin effect, NMR experiments on metals require either powder samples or samples made from thin foils. Up to now, the majority of NQDOR measurements including the measurements on irradiated copper by Minier et al. [11] employed powder samples, which give better signal/noise ratios. Since in the present approach measuring NQDOR and electrical resistance on the same sample was mandatory, samples consisting of an assembly of thin foils were used. This had the additional advantage that the samples could be irradiated fairly homogeneously. Well-defined cold-working and quenching experiments are possible only on foils.

In the present work we used Cu foils prepared from Johnson-Matthey or Leico 5N copper, and Be-doped foils (Cu/200 ppm Be) that were prepared by melting a 5 mm copper rod with an inlayed 50 μm Be wire. After rolling, the foils were electropolished in order to remove impurities at the surfaces and subsequently annealed at 700 K (the foils intended for cold-work at 750 K) for one hour. Copper wires for resistance measurements were spot-welded to the foils used for electron irradiations. The other samples were connected to the wires by means of clamps after the introduction of the intrinsic point defects.

Electron and proton irradiations were performed at the Dynamitron accelerator of the Institut für Strahlenphysik of Stuttgart University at temperatures between 80 and 130 K. For the proton irradiation a special sample holder was built that fitted into the irradiation chamber originally designed for the electron irradiation. It permitted a direct connection of the sample to the beam line, using the sample foil as partition wall between l-N_2 and the vacuum of the beam line. (In the e^- irradiation set-up the e^- have to pass through about 4 mm of the cooling medium l-N_2, which in the case of proton irradiation would have caused an unacceptably high energy loss.)

The NMR samples were assembled in a l-N_2 bath without warming up. The foils were electrically iso-

lated by thin mica foils, or by quartz plates when annealing at higher temperatures was intended. The vessel for the foils and the sample holder with the r.f. coil were made from the same glass-ceramics (Macor™) in order to ensure that they fit together even at low temperatures.

4.3.2 The Experimental Procedure

The experimental procedure is illustrated in Figure 7. After introducing the intrinsic point defects at low temperatures by irradiation or cold-work, the NMR samples were assembled as described above, inserted into the sample holder, and transferred to the cryostat without warming them up. Measurements of the spin–lattice relaxation time in zero applied field, T_1^{zero}, of NQDOR spectra, and of the electrical resistance were followed by isochronal (600 s) anneals at increasing temperatures. The resistance was measured after each annealing step, while the NQDOR spectra were obtained only after annealing treatments during which significant resistivity changes had occurred. NQDOR measurement after each annealing step would have been too time-consuming.

4.3.3 Analysis of NQDOR Data

A weak structureless absorption observed in the lower DIT regime appears with DIT as well as under r.f. irradiation with a *single* frequency if the amplitude B_1^{NQR} is made as large as the one used in DIT (see Figure 8). Together with the fact that under these conditions the well-resolved DIT lines disappear this indicates clearly that the background absorption is not caused by EFG corresponding to this frequency range. The background is presumably due to the enhancement of the high-frequency wing of the strong dipolar and quadrupolar absorption near B_L induced by the high B_1^{NQR} values required for DIT. Therefore the low-frequency background in the DIT measurements may contain quadrupolar contributions arising from lines at very low frequencies. Since these may depend on the defect pattern, in each DIT measurement the background must be substracted separately. The background could be approximated by an exponential dependence of the absorption from the frequency. This function was fitted to those data points which were clearly not affected by NQDOR lines (referred to as base points). Figure 9 demonstrates this for the example of a dilute alloy of copper with

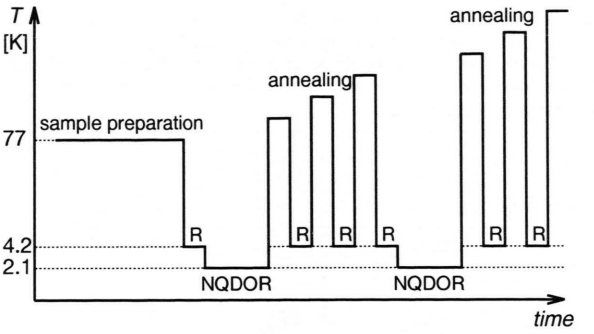

Fig. 7. The course of an NQDOR experiment on intrinsic point defects. R = measurement of the electrical resistance.

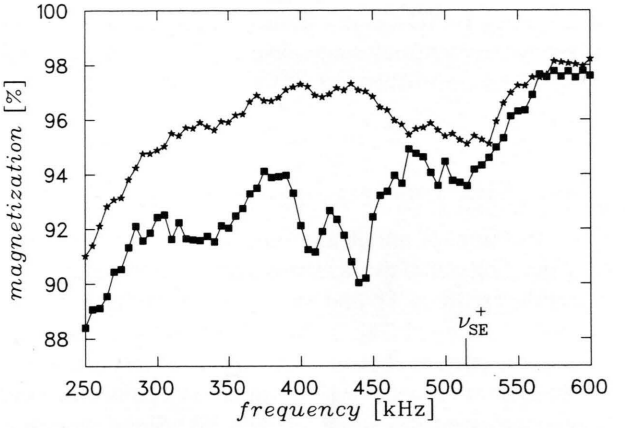

Fig. 8. Two NQDOR spectra of a cold-worked copper sample (not annealed), obtained in the DIT regime using r.f. irradiation with a single frequency (★) or with normal DIT (■) at equal B_1^{NQR} levels. Single irradiation shows only a continuous background, except for the Solid-Effect transition at ν_{SE}^{+} (cf. Section 2.4).

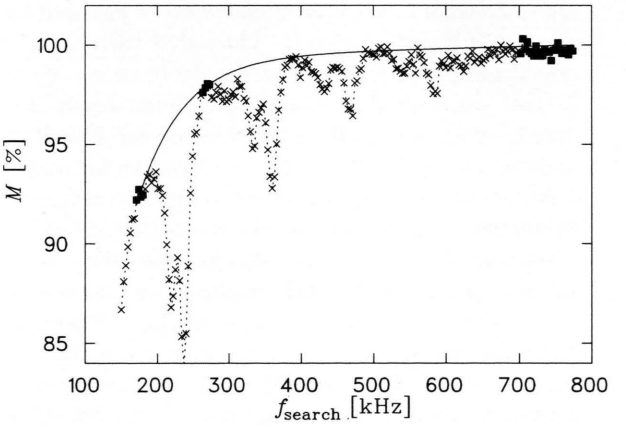

Fig. 9. Background determination on the example of an NQDOR spectrum of Cu/200 ppm Be (×). The function $M = 100 - A \exp(-B f_{search})$ (—) was fitted to points not affected by NQDOR lines (■). M = magnetization, f_{search} = search frequency, A and B fit parameters.

Table 3. Frequencies and relative intensities of the line pairs due to Be atoms in a dilute Cu/200 ppm Be alloy in the DIT and SIT regimes. Since the lines at 65 kHz, 113 kHz, and 129 kHz are very weak, their frequencies are only approximate. The 45 kHz line consists of at least two different overlapping transitions. The r.f. amplitude B_1^{NQR} in the DIT was 1.6 mT.

Detection regime			DIT		
$\nu_q(^{63}Cu)$/kHz	2049.3 ± 0.1	583.7 ± 0.8	467.7 ± 0.7	360.0 ± 0.4	237.22 ± 0.2
$\nu_q(^{65}Cu)$/kHz	1896.3 ± 0.2	539.5 ± 1.5	430.9 ± 1.1	333.3 ± 0.6	219.0 ± 0.3
Rel. line intensity	0.43	0.19	0.27	0.52	1
Detection regime			**SIT**		
$\nu_q(^{63,65}Cu)$/kHz	≈129	≈113	≈83	≈65	≈45

200 ppm Be. The continuous background absorption of spectra without point-defect lines could be fitted with this approach, too.

4.4 Results

4.4.1 Electron Irradiation of Cu/Be

Addition of small amounts of Be suppresses the annealing out of those intrinsic defects (crowdion-type self-interstitials [1]) that in pure copper migrate in the recovery Stage I [26]. In Stage-II irradiations, as in the present case, the ensuing reduction of instantaneous interstitial–vacancy recombination enhances the damage rate considerably [27, 28]. Since for each trapped self-interstitial an additional vacancy is retained in the lattice, doping by Be will affect the intensities of the irradiation-induced lines if some of them are due to vacancies and others to self-interstitials. Under the present conditions the intensity ratios of self-interstitial to vacancy lines should be changed by more than a factor of three compared with the undoped sample [27]. Furthermore, the trapping of the Stage-I_E interstitials by Be atoms should result in a drastic reduction in the intensities of the NQDOR lines which are due to the Be in the copper lattice (cf. Table 3). The Be–self-interstitial complexes created by the trapping might even give rise to additional lines.

Irradiation of the Cu/200 ppm Be alloy with $1.7 \cdot 10^{23}$ e^-/m^2 at 2.5 MeV resulted in an increase of the residual electrical resistivity of $\Delta\varrho_0 = 300$ pΩm. This corresponds to a Frenkel-pair concentration $C_{FP} = 12 \cdot 10^{-4}$ if a resistivity $\varrho_{FP} = 2.5$ μΩm per unit concentration of Frenkel pairs is assumed [29]. After annealing at 590 K the NQDOR spectrum was indistinguishable from that of the non-irradiated sample (cf. Fig. 10, top). The lines in this spectrum are attributed to EFG in the neighbourhood of substitutional

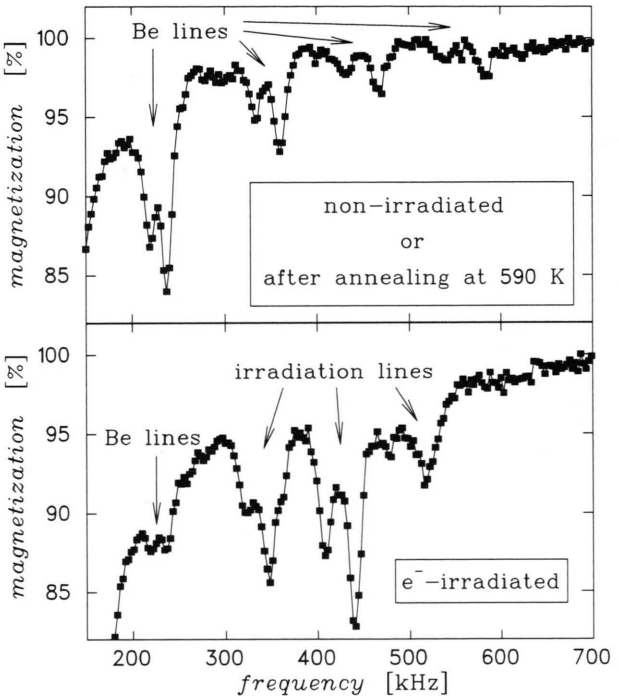

Fig. 10. Be-doped sample: NQDOR spectra in the lower DIT regime before (top) or after (bottom) e^- irradiation.

Be atoms. (The phase diagram of the binary alloy Cu/Be shows a Hume-Rothery-type α-phase at low Be concentrations. It is unlikely that interstitial Be that might be present in addition to substitutional Be would give rise to lines whose intensity is comparable with that of substitutional lines.) Table 3 gives the frequencies of these "Be lines". Note that besides the lines visible in Figs. 10 and 11 additional lines exist in the MHz range and at frequencies below about 200 kHz in the SIT range. A search for SE lines was not performed.

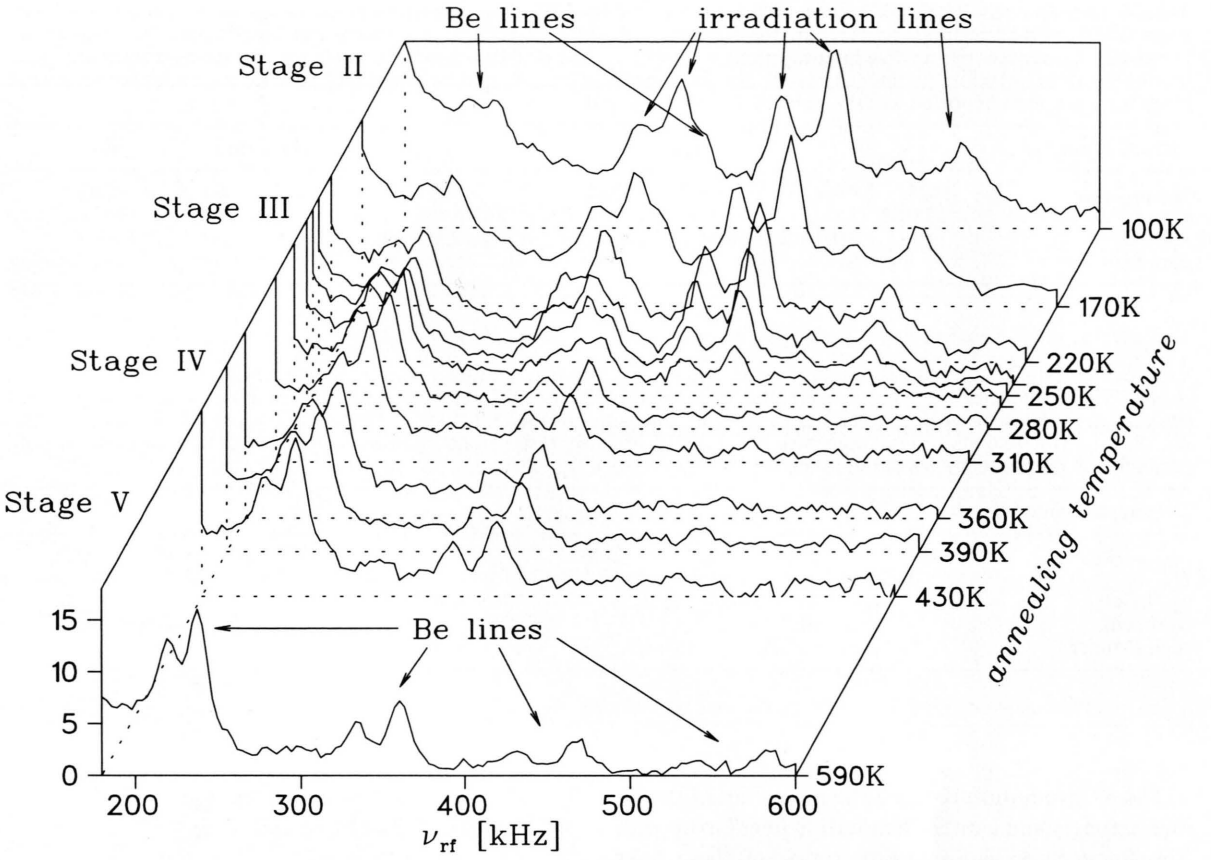

Fig. 11. Be-doped sample: NQDOR spectra in the lower DIT regime as obtained after annealing at the indicated temperatures.

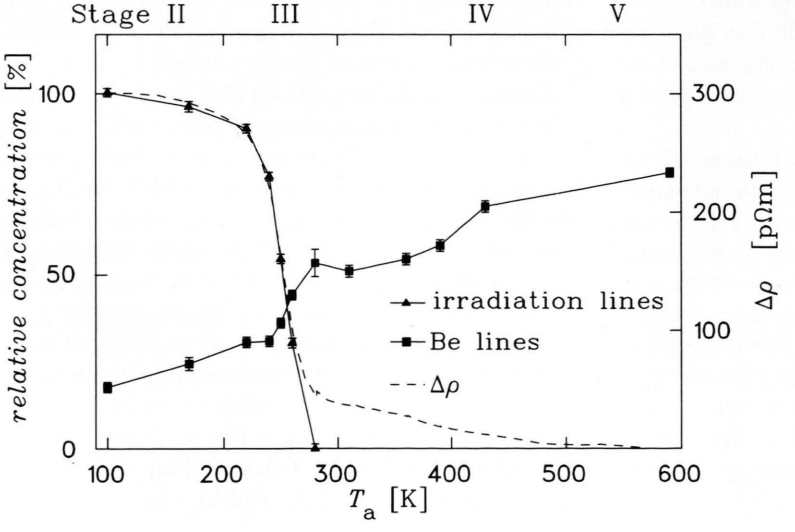

Fig. 12. The variation of the residual electrical resistivity and of the strongest pairs of the Be lines (at 237 kHz) and of the irradiation lines (at 347 kHz and 440 kHz) (expressed as relative concentrations) with the annealing temperature T_a.

Table 4. Data from the NQDOR spectra of a dilute Cu/200 ppm Ni alloy. The frequencies $\nu_{SIT,DIT}$ have been obtained with normal SIT or DIT; the frequencies ν_{SE} are those of the newly detected SE transitions (here and later on only ^{63}Cu transitions are given). I_{rel} denotes the relative intensities of the DIT lines. The DIT lines below 200 kHz are affected by additional direct cross-relaxation, therefore no intensity ratios are given for these lines. *: in the normal DIT spectra these lines are very weak (they were not even reported as DIT lines by Minier et al. [9]).

Detection regime	DIT				DIT/SIT		SIT
$\nu_{SIT,DIT}$/kHz	1125	*	224	*	≈145	≈125	≈40
I_{rel}	0.38	–	1	–	–	–	–
ν_{SE}/kHz		260 (=220+40)		180 (=220−40)			
comment		SE^+		SE^-			overlapping

Table 5. The NQDOR "irradiation" lines as detected after low-temperature electron/proton irradiation or cold-work of copper. The frequencies $\nu_{SIT,DIT}$ are observable with ordinary SIT or DIT, the frequencies ν_{SE} are those of the SE transitions detected in the present work. I_{rel} denotes the relative intensities of the DIT lines. [a]: Minier et al. reported 3425 kHz for this line [9, 11], [b]: the line may be not seen with normal DIT because it is overlaid by other lines, [c]: assignment to shells around vacancies as proposed by Minier et al. [9, 11].

Detection regime	DIT				SIT		
$\nu_{SIT,DIT}$/kHz	3438[a]	515	440	[b]	347	≈85	≈75
I_{rel}	0.35	0.41	1	–	0.59	–	–
ν_{SE}/kHz		515 (=440+75)		365 (=440−75)			
comment		SE^+		SE^-		overlapping	
shell (Minier)[c]	1	2 (!)	3		4	5	7

The e^- irradiation reduced the intensities of the Be lines strongly and caused "irradiation lines" to appear. The frequencies and intensity ratios of these lines agreed with those observed on e^--irradiated undoped copper by Minier et al. [9, 11] and in our work (cf. Fig. 13 and Table 5). No hitherto unknown lines were found in spite of intense search over the frequency range from 20 kHz to 4 MHz. (As mentioned above, the spectra shown in Figs. 10 and 11 include only part of the total frequency range scanned. This holds for the spectra of pure Cu containing intrinsic point defects and in Cu doped with Ni, too, cf. Tables 4 and 5.)

Figures 11 and 12 survey the variations of the NQDOR spectra during a sequence of annealing treatments. In agreement with the results of Minier et al. [11], in Stage III the irradiation lines became unobservably small. From this we deduce that after Stage III not more than 2% of the initial concentration of the defects responsible for the irradiation lines in e^--irradiated pure Cu remain while 16% of $\Delta\varrho_0$ is retained (dashed line in Figure 12). In agreement with the electrical resistivity, the Stage-III recovery of the Be lines is only partial; complete recovery does not take place till Stage V.

4.4.2 Defect Generation in Cu by Different Techniques

The present work employed three different methods to introduce intrinsic point defects into Cu at low temperatures, viz. e^- irradiation, proton irradiation, and cold-work. These three methods are expected to result in different defect patterns. Beforehand it was not clear whether in the NQDOR spectra the intrinsic point defects could be separated from other defects such as dislocations and defect clusters.

Electron irradiation of Cu with $1.2 \cdot 10^{23}$ e^-/m^2 at 3 MeV resulted in an increase of the residual electrical resistivity of $\Delta\varrho_0 = 48$ pΩm ($C_{FP} \approx 20$ ppm), proton irradiation with $5 \cdot 10^{20}$ p/m^2 at 3 MeV in $\Delta\varrho_0 =$ 500 pΩm ($C_{FP} \approx 200$ ppm). The cold-worked sample was rolled at about 77 K to a thickness reduction of 67%, yielding $\Delta\varrho_0 = 2.1$ nΩm. Since in this case dislocations are known to contribute significantly to $\Delta\varrho_0$, no Frenkel-pair concentration is given. All three spectra showed the same lines with essentially the same intensity ratios (cf. Fig. 13), whereas the ratio of the line intensities to $\Delta\varrho_0$ is much smaller in the proton-irradiated and the cold-worked samples than in the e^--irradiated sample. Line widths and continuous

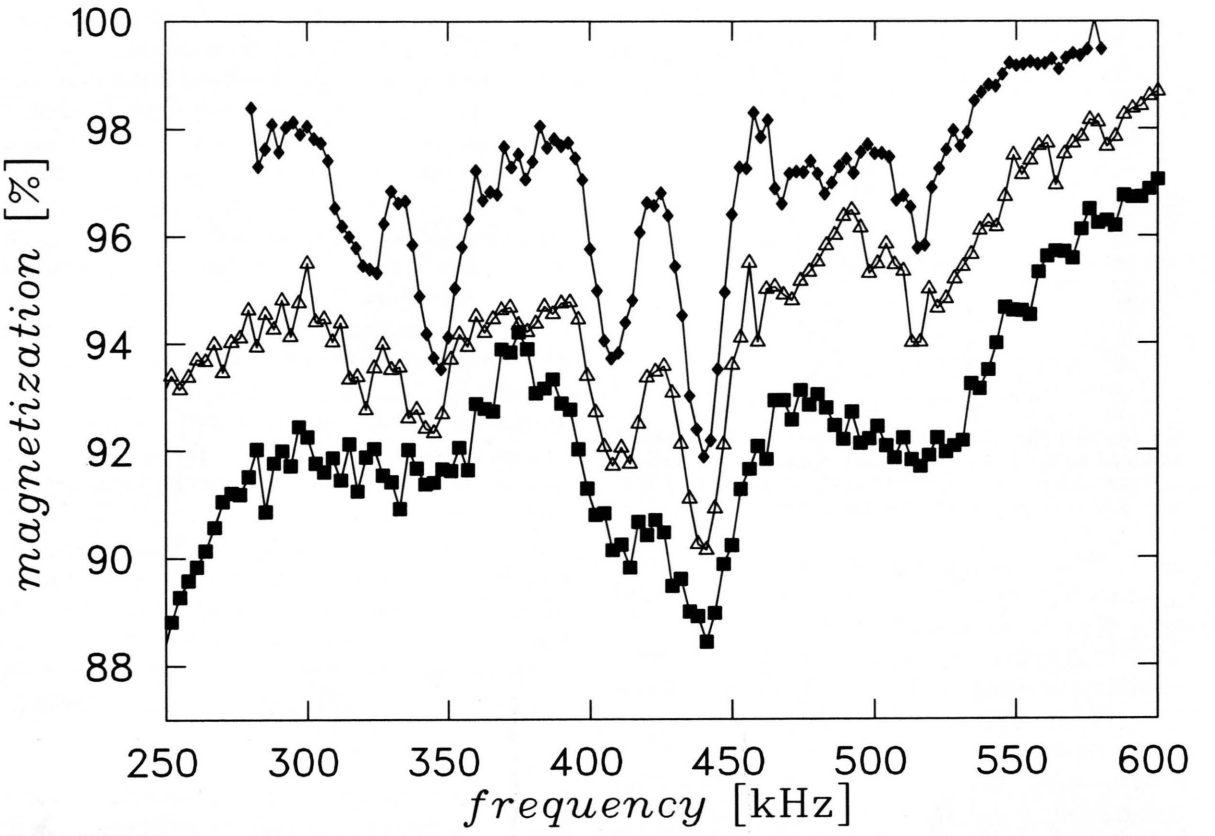

Fig. 13. NQDOR spectra of an e^--irradiated (◆), a proton-irradiated (△), and a cold-worked sample (■), as measured before any annealing.

background increased in the sequence e^- irradiation, proton irradiation, cold-working. After all pre-treatments the lines became invisible during Stage-III annealing.

Pilot experiments on Cu foils that were quenched from the melt by either melt-spinning or splat-cooling did *not* reveal any NQDOR lines which could be attributed to intrinsic point defects. This result appears to be highly significant since in this type of treatment we expected *vacancies* and *not* interstitials to be frozen in. A more detailed account of these experiments will be published elsewhere [30].

4.4.3 Demonstration of the Solid Effect in Cu and Cu/Ni

Minier et al. [10] reported experimental evidence for NQDOR SE lines in electron-irradiated Al but did not investigate them in detail. Solid-Effect lines in Cu were not reported previously. Using the special r.f.-irradiation techniques in zero applied magnetic field described in Sect. 2.4, we found SE transitions in copper containing 200 ppm nickel and in both cold-worked and proton-irradiated copper (cf. Tables 4 and 5). In Fig. 14 this is illustrated on a proton-irradiated Cu sample that had been annealed at 220 K, i.e. just below Stage III. It was irradiated in zero field with two frequencies of widely different amplitudes, viz. with the frequency $f_S = 440$ kHz and amplitude $B_1 = 0.28$ mT in order to saturate the S transition at that frequency (cf. Fig. 13 for the "normal" DIT spectrum of a proton-irradiated sample) and a variable frequency f_{search} of amplitude $B_1 = 1.4$ mT. When f_{search} coincides with the SE frequencies ν_{SE}^+ or ν_{SE}^- [cf. Eq. (6)] an enhanced absorption (strong drop in the magnetization) should occur, yielding the butterfly pattern typical for this kind of SE detection. For the irradiation lines in copper this was observed at $\nu_{\text{SE}}^+ = 365$ kHz and $\nu_{\text{SE}}^- = 515$ kHz for ^{63}Cu. Note that SE transitions are possible for all combinations of ν_I

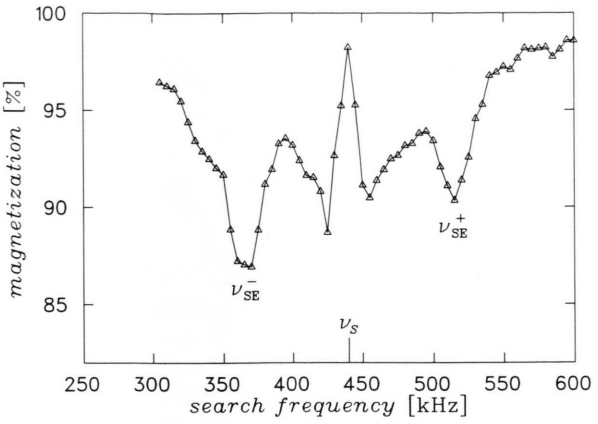

Fig. 14. Solid Effect illustrated on a proton irradiated sample annealed at 220 K (i.e., just below Stage III). ν_{SE}^{+} and ν_{SE}^{-} indicate SE transitions associated with the line at ν_S. The r.f. irradiation conditions are explained in the text.

and ν_S which arise from isotopes with different nuclear quadrupole moments. In our example the contributions of ν_S at 407 kHz (^{65}Cu) and 440 kHz (^{63}Cu) could be experimentally separated whereas the two ν_I transitions at about 75 kHz gave rise to a broadening of the observed SE transitions.

The structure visible in Fig. 14 between 400 and 480 kHz is an artifact of the specific r.f. irradiation technique employed. It demonstrates the characteristics of the various irradiation techniques: During the scan for SE transitions conditions similar to normal DIT arise when $|f_S - f_{\text{search}}| \approx 15$ kHz, yielding the wings of the DIT line normally seen at ν_S. Only when f_{search} becomes nearly equal to the second applied frequency f_S (at ν_S) do we observe a sharp increase of the magnetization, since now the situation is equivalent to an SIT irradiation.

4.5 Discussion

4.5.1 NQDOR Data and Line Assignments

As mentioned, under the present irradiation conditions the Be doping employed in this paper increases the ratio of isolated interstitials to vacancies by more than a factor of 3. Hence we can conclude from the doping independence of their intensity ratios that all strong irradiation lines must be caused by the same defect. This *v* indicates an assumption made without experimental proof by Minier et al. [9–11] and is consistent with the results obtained on the differently pretreated samples. With the exception of the quenching from high temperatures none of the different methods employed to create intrinsic point defects yielded spectra that differed significantly from the others in spite of the fact that the ratios of isolated interstitials and isolated vacancies were presumably quite different.

Independently of the arguments of the preceding paragraph the demonstration that the 515 kHz line is a SE line proves that the quadrupolar splittings giving rise to the lines at 75 kHz and 440 kHz are due to the same defect. The nuclei involved are presumably nearest neighbours. This should help in the final assignment of the lines. The following two statements may be made at the present stage: (i) The shell assignment by Minier et al. [9–11], who thought that all irradiation lines were due to monovacancies, cannot be maintained since the 515 kHz transition does not correspond to an EFG. (ii) Since the shells around ⟨100⟩ dumbbells may give rise to two EFG values and since there is a zeroth shell, the assignment of the EFG associated with the irradiation lines to self-interstitials (see below) involves fewer shells than the Minier assignment. E.g., five distinct lines may be accommodated in the shells $n = 0, 1, 2$, whereas in the case of vacancies shells at least up to $n = 5$ were required.

We have not found lines that might be attributed to the clusters formed by trapping of interstitials at the Be atoms during the e^- irradiation of the dilute Cu/Be alloy. This is not too surprising since a fairly wide variety of such clusters should be formed and the symmetry of most of them should be rather low. We therefore expect them to contribute to the background absorption. Nevertheless, we were able to derive information on the clusters from the recovery of the Be lines during annealing (cf. Fig. 12), as will be shown elsewhere.

The results on the cold-worked sample demonstrate that intrinsic point defects are observable by NQDOR even in highly defective crystals containing large densities of other defects. These make themselves felt by increased line widths due to inhomogeneous line broadening and an increased background.

In agreement with the findings of Minier et al. [11], after Stage-III no irradiation lines were visible on all samples, while a significant fraction of the additional residual resistivity $\Delta\varrho$ remained. This indicates strongly that the defects responsible for the strong irradiation lines are *not* the same as those giving rise to the irradiation-induced resistivity remaining after Stage-III annealing. It is unlikely that the "NQDOR defects" are vacancies since then the lines should have

shown up in the quenching experiments referred to at the end of Section 4.4.2. This conclusion is at variance with the computations of Drittler et al. [21] referred in Sect. 4.2, which predict the quadrupolar transition frequency at the nearest neighbours of vacancies in Cu to be about 6 MHz. Even if such a rather high frequency should have escaped detection in the present experiments, in the frequency range thoroughly searched by us there should have been transitions at more distant neighbours of the vacancies. Such transitions have not been found. The reason for this discrepancy between experiment and computation is not yet known.

The similarity of the Cu and Al results suggests that the irradiation lines in Al are *not* due to vacancies either. In this case the absence of NQDOR lines attributable to vacancies is in agreement with the theoretical results of Furthmüller [22] (cf. Section 4.2).

On the basis of the evidence discussed so far, the strongest candidates for the defects responsible for the well-developed irradiation lines are clearly self-interstitials that migrate in Stage III. Rather strong support for this viewpoint comes from the observations on e^--irradiated Cu/200 ppm Be to be briefly discussed in the next section and to be expounded more fully elsewhere.

4.5.2 Comparison of NQDOR and Electrical Resistivity Results

As mentioned in Sect. 4.1, one approach to a definite assignment of the NQDOR lines is the comparison with data obtained by other techniques. We illustrate this by considering the recovery of the "irradiation lines" as observed on the Cu/200 ppm Be sample after low-temperature electron irradiation (Fig. 12) with that of the electrical resistivity measurements on the same sample.

A key problem in the interpretation of radiation-damage experiments on metals is that in most fcc and bcc metals, among them Cu and its dilute alloys, there are *two* recovery stages that show all the features of a defect–antidefect annihilation reaction between the elementary intrinsic point defects, i.e., between vacancies and self-interstitials. By tradition these stages are called I_E (in Cu at about 55 K) and III (in Cu at about 250 K). In the course of time many explanations for this "Stage-III dilemma" have been proposed. Most of them have fallen into oblivion. The explanations which are still in use belong to one of two broad categories which have become known under the names two-interstitial model [1] and one-interstitial model [2].

The two-interstitial model resolves the Stage-III dilemma in a very simple manner by stating that in the metals showing Stage-I_E recovery (Au does not!) in addition to Stage-III recovery (which possesses the same features in *all* fcc metals and therefore appears to be the more "basic" of the two stages in question) *two* mechanically stable self-interstitial configurations may exist. Stage-I_E recovery is attributed to the migration of so-called crowdions, which migrate one-dimensionally (in fcc metals along the ⟨100⟩ directions), Stage-III recovery to the (three-dimensional) migration of the ⟨100⟩ dumbbells (cf. Section 4.1). The crowdion configuration is assumed to be metastable with respect to the ⟨100⟩ dumbbell configuration and can be converted into the latter, e.g. by intense irradiation.

The one-interstitial model attributes the Stage-III reaction of the two-interstitial model (i.e., the annihilation of vacancies by three-dimensionally migrating ⟨100⟩ dumbbell interstitials) to Stage I_E. (This creates a serious difficulty in such cases as Au, where Stage I_E has not been found in spite of intense efforts.) Hence, for Stage III another explanation must be found. For this a number of proposals have been made in the course of time, the most popular being that in Stage III vacancies migrate towards self-interstitial clusters that had been formed at lower temperatures.

Both models have in common that vacancies migrate more slowly than self-interstitials. Both account for the complete disappearance (within experimental accuracy) of the NQDOR lines in Stage III by attributing them to the defects migrating in that stage, i.e., to ⟨100⟩ dumbbell self-interstitials in the case of the two-interstitial model and to vacancies in the case of the one-interstitial model. As we have seen, these two interpretations cannot be distinguished easily by considering the intensity ratios of the NQDOR lines (cf. Section 4.1). A distinction is possible, however, by comparing the line intensities with measurements of the electrical resistivity. The decisive difference between the two models is that in the two-interstitial model the vacancy–self-interstitial recombination process ceases to be the dominant process when the vacancy concentration has become so low that the majority of the migrating dumbbells react no longer with vacancies but with interstitial clusters, dislocations etc. This accounts for the observation that at the end of Stage III the recovery of the resistivity does no

longer follow that of the NQDOR line intensity (cf. Section 4.4.1). By contrast, according to the one-interstitial model the same process takes place throughout Stage III, viz. the migration of vacancies towards interstitial clusters and the formation of vacancy clusters. The model can therefore not explain why over most of Stage III NQDOR lines and resistivity recover in parallel while after a certain point the two quantities behave quite differently.

5. Conclusions

Nuclear Quadrupole Double Resonance has been shown to be a powerful tool for studying intrinsic defects in metals even if their concentration is low. Judged from the comparison with electrical-resistivity data point-defect concentrations as low as a few ppm can be detected. Considerable progress has been achieved in the assignment of NQDOR lines as "fingerprints" of such defects, in particular in the identification of so called "Solid-Effect lines". In contrast to "normal" NQDOR lines, the SE lines do not correspond to individual electric field gradients but give information on the positions of the atoms surrounding the defects.

The weakness of the NQDOR technique is that it is confined to a rather small number of metals. The specific application of the NQDOR technique to copper and dilute copper alloys shows that all EFG appearing after low-temperature irradiation by electrons or protons are due to the same defect, which is identified as the ⟨100⟩ dumbbell self-interstitial. In the accessible frequency range of about 2.5 decades no indications of vacancy lines have been found. Presumably the electric field gradients generated by the vacancies at their neighbour sites are too small to gives rise to well separated NQDOR lines. Taken together with measurements of the electrical resistivity the recovery of the NQDOR lines supports the two-interstitial model rather than the one-interstitial model of radiation damage in fcc metals.

Acknowledgement

The technical assistance of the staff of the Dynamitron accelerator at Stuttgart University during the particle irradiation and the help and advice we have received in specimen preparation and during the measurements from the personnel of the Max-Planck-Institut are gratefully acknowledged. The authors would also like to express their thanks to Professor M. Fähnle and his collaborators for providing valuable information on the calculation of electric field gradients in metals.

[1] A. Seeger, in: Fundamental Aspects of Radiation Damage in Metals (M. T. Robinson and F. W. Young Jr., eds.), Gatlinburg, Tenn., USA, US ERDA Conf. –751006-P1, 1975, p. 493.
[2] W. Schilling, P. Ehrhart, and K. Sonnenberg, in: Fundamental Aspects of Radiation Damage in Metals (M. T. Robinson and F. W. Young Jr., eds.), Gatlinburg, Tenn., USA, US ERDA Conf. –751006-P1, 1975, p. 470.
[3] N. F. Ramsey and R. V. Pound, Phys. Rev. **81,** 278 (1950).
[4] A. G. Redfield, Phys. Rev. **130,** 589 (1963).
[5] R. E. Slusher and E. L. Hahn, Phys. Rev. **166,** 332 (1968).
[6] M. Minier, Phys. Rev. **182,** 437 (1969).
[7] D. T. Edmonds, Phys. Reports (Phys. Lett. C) **29,** 233 (1977).
[8] M. Blanz, M. Hampele, G. Majer, M. Notter, and A. Seeger, in: Congress Ampere on Magnetic Resonance and Related Phenomena (M. Mehring, J. U. Schütz, and H. C. Wolf, eds.), Springer Verlag, Berlin, Stuttgart 1990.
[9] M. Minier and C. Minier, Phys. Rev. B **22,** 21 (1980).
[10] M. Minier, C. Minier, and R. Andreani, Phys. Rev. B **18,** 102 (1978).
[11] M. Minier, C. Minier, and R. Andreani, Phys. Rev. B **22,** 28 (1980).
[12] P. Pyykkö and J. Li, Report HUKI 1-92, Helsinki (1992) (ISSN 0784-0365). P. Pyykkö and J. Li, NQR Newsletter **1** (2), 19 (1993).
[13] M. H. Cohen, Phys. Rev. **96,** 1278 (1954).
[14] H. Chihara and N. Nakamura, in: Nuclear Quadrupole Resonance Spectroscopy Data (K. H. Hellwege and A. M. Hellwege, eds.), Landolt-Börnstein, Springer-Verlag, Berlin 1988, NS III/20 a–c.
[15] S. R. Hartmann and E. L. Hahn, Phys. Rev. **128,** 2042 (1962).
[16] M. Goldman, Spin Temperature and Nuclear Magnetic Resonance in Solids, Clarendon Press, Oxford 1970.
[17] Cl. Berthier and M. Minier, Phys. Rev. B **7,** 1854 (1973).
[18] A. Seeger, E. Mann, and R. v. Jan, J. Phys. Chem. Solids, **23,** 639 (1962).
[19] H.-G. Haubold and D. Martinsen, J. Nucl. Mat. **69–70,** 644 (1978).
[20] M. J. Ponnambalam, Z. Naturforsch. **47a,** 45 (1992).
[21] B. Drittler, M. Weinert, R. Zeller, and P. H. Dederichs, Phys. Rev. B **42,** 9336 (1990).
[22] J. Furthmüller and M. Fähnle, MPI für Metallforschung, Stuttgart, personal communication, 1992.
[23] P. Blaha, K. Schwarz, and P. H. Dederichs, Phys. Rev. B **37,** 2792 (1988).
[24] R. Pawellek, Dr. rer. nat. thesis, Universität Stuttgart, Stuttgart, Germany, 1991.
[25] R. Pawellek, M. Fähnle, C. Elsässer, K.-M. Ho, and C.-T. Chan, J. Phys.: Condens. Matter **3,** 2451 (1991).
[26] A. C. Baily, W. E. King, and K. L. Merkle, Phys. Rev. B **46,** 8593 (1992).
[27] J. Bewerunge, Dr. rer. nat. thesis, Technische Hochschule Aachen, Aachen, Germany, 1979.
[28] A. Bartels, J. Bewerunge, F. Dworschak, and H. Wollenberger, J. Phys. F, **12,** 641–648 (1992).
[29] P. Ehrhart, P. Jung, and H. Schultz, in: Atomic Defects in Metals (H. Ullmaier, ed.), Landolt-Börnstein, Springer-Verlag, Berlin 1991, NS III/25, Sect. 2.3.2.
[30] K. Konzelmann, G. Majer, M. Notter, and A. Seeger, to be published.